Carbohydrate Polymers 84 (2011) 1141–1150

Contents lists available at ScienceDirect

Carbohydrate Polymers

journal homepage: www.elsevier.com/locate/carbpol

In situ SAXS under shear unveils the gelation of aqueous starch suspensions and the impact of added amylose–lipid complexes

J.A. Putseys[a], C.J. Gommes[b,d], P. Van Puyvelde[c], J.A. Delcour[a], B. Goderis[d,*]

[a] *Laboratory of Food Chemistry and Biochemistry and Leuven Food Science and Nutrition Research Centre (LFoRCe), Katholieke Universiteit Leuven, Kasteelpark Arenberg 20, B-3001 Heverlee, Belgium*
[b] *Department of Chemical Engineering, Université de Liège, Allée du 6 août B6a, B-4000 Liège, Belgium*
[c] *Department of Chemical Engineering, Katholieke Universiteit Leuven, W. de Croylaan 46, B-3001 Heverlee, Belgium*
[d] *Chemistry Department, Katholieke Universiteit Leuven, Celestijnenlaan 200F, B-3001 Heverlee, Belgium*

ARTICLE INFO

Article history:
Received 17 September 2010
Received in revised form 4 January 2011
Accepted 5 January 2011
Available online 12 January 2011

Keywords:
Starch
Rheology
Small angle X-ray scattering
Gelation

ABSTRACT

The gelation of heat-treated, aqueous starch suspensions has been explained either in terms of a nanoscopic amylose aggregation or a fractal-like phase separation. These concepts, as well as the supporting experimental evidence, at first sight seem incompatible. The present study exploits rheometry in combination with *in situ* small angle X-ray scattering and clearly points to creation of finely dispersed, elongated nano-objects when a starch gel is formed in the presence of shear forces. These objects are interpreted as aggregated amylose double helices that provide the system with physical, intermolecular crosslinks. Increasing the aggregate size and concentration increases the gel storage modulus. The gelation process is enhanced in the presence of amylose–lipid complexes as, during heating, short amylose fragments are liberated from these complexes that, upon cooling, promote amylose aggregation and thus gel formation. When shearing is stopped, the aggregates promptly grow and agglomerate into larger fractal objects resulting in an increased gel stiffness. The present work thus suggests that small scale amylose aggregation and the formation of fractal phases have to be considered as subsequent events rather than as mutually exclusive concepts. Finally, it is argued that size-induced polymorphic changes may also contribute to the starch gel stiffness.

1. Introduction

Native starch occurs in the form of partly crystalline granules that mainly consist of amorphous amylose and semicrystalline amylopectin. Amylose, the smaller of the two polymer fractions (around 25%), is predominantly linear, whereas amylopectin (around 75%) is highly branched (Buléon, Colonna, Planchot, & Ball, 1998; Tester, Karkalas, & Qi, 2004). Next to being the major energy source in the human diet, starch is also an important determinant in the texture of foods (Wang, Bogracheva, & Hedley, 1998) such as mashed potatoes and bakery products.

In their natural form at room temperature, starch granules are not soluble in water and, in the absence of external forces, precipitate from aqueous solutions. In excess water, temperatures above the gelatinization temperature induce irreversible changes leading to swollen, and even disrupted starch granules (Delcour et al., 2010; Delcour & Hoseney, 2010). The gelatinization temperature is defined as that at which starch granules lose their birefringence. They swell, amylopectin crystals melt, and amylose gains mobility and leaches out of the granules (Jenkins & Donald, 1998; Tester & Debon, 2000; Waigh, Gidley, Komanshek, & Donald, 2000).

All events that occur during heating beyond the loss of birefringence are collectively referred to as pasting (Delcour & Hoseney, 2010). During pasting, a strong viscosity increase of the starch dispersion is noted first (Atwell, Hood, Lineback, Varriano-Marston, & Zobel, 1988), which decreases again upon further heating. This rheological complexity can be explained by the interplay of granule swelling, granule rigidity and amylose leaching (Delcour & Hoseney, 2010; Juhasz & Salgo, 2008; Tester & Morrison, 1990). In the process, at a sufficiently high starch concentration, the swelling granules may impinge at a given temperature and ultimately fill the space completely. At that stage, the system viscosity is predominantly determined by the granule rigidity (Steeneken, 1989). Shear forces promote the homogenisation into a uniform starch paste. Cooling of the hot starch paste causes the viscosity to increase again and produces a gel, the formation and structure of which are relevant to, *e.g.* the thickening of soups and sauces as well as glue systems, and which is the subject of the present paper.

Gelation has frequently been studied by analysis of amylose suspensions, which are molecularly less complex than starch sus-

---

* Corresponding author. Tel.: +32 016 327806; fax: +32 016 327990.
E-mail address: bart.goderis@chem.kuleuven.be (B. Goderis).

0144-8617/$ – see front matter © 2011 Elsevier Ltd. All rights reserved.
doi:10.1016/j.carbpol.2011.01.003

pensions. Miles, Morris, Orford, and Ring (1985) and Miles, Morris, and Ring (1985) attributed gelation of amylose systems during cooling to phase separation of the homogenized matrix into a polymer-rich and a polymer-deficient (*i.e.* water-rich) region. Although crystallization of amylose by aggregation of the earlier formed amylose double helices might take place within the polymer-rich phase, these authors suggested that phase separation on its own could be responsible for gelation.

The secondary role of crystallization was challenged by I'Anson, Miles, Morris, and Ring (1988). They investigated the gelation process in amylose solutions with combined synchrotron small angle X-ray scattering (SAXS) and wide angle X-ray diffraction (WAXD). As the SAXS patterns did not reveal any features that could be associated with phase separation, it was argued that the large phases scattered outside the SAXS angular window. Only smaller, phase-internal features were in view right from the start of gelation, which were identified as rod-like crystallites. However, their crystalline nature is rather speculative since only after a considerable time B-type diffraction patterns were observed in WAXD. Similar observations were made by Imberty and Perez (1988). Interestingly, the nano-object concentration in the work by I'Anson et al. (1988) increased during the course of gelation, parallel to the increase in shear modulus.

Later, Gidley and Bulpin (1989) and Leloup, Colonna, Ring, Roberts, and Wells (1992) followed this line of thought and argued that small solid aggregates of amylose double helices – acting as intermolecular junctions – are directly responsible for gelation. In contrast, Vallera, Cruz, Ring, and Boué (1994) studied amylose gelation in deuterated water with small angle neutron scattering (SANS) and concluded that their data – covering the same scattering vector range as in the SAXS work by I'Anson et al. (1988) – could *only* be interpreted as resulting from the presence of two 'homogeneous' phases: one being almost pure deuterated water, the other being polymer-rich and displaying a fractal structure. The fractal aggregates themselves were estimated to span over several micrometers, which is consistent with a turbidity to visible light.

Literature on the principles governing the gelation of aqueous amylose suspensions thus presents seemingly incompatible arguments in favour of either nanoscopic amylose aggregation/crystallization or fractal-like phase separation with morphological features up to μm length scale.

This ambiguity also exists in the literature dealing with the gelation of starch suspensions, which – at least at the early stage of the process – is believed to be dominated by the amylose fraction. According to Miles, Morris, and Ring (1985), irreversible amylose–amylose interactions take place quickly after cooling (few minutes to few hours), and result in a starch gel. In contrast, retrogradation of amylopectin with recrystallization of its side chains only occurs over a period of several days (Atwell et al., 1988; Miles, Morris, Orford, et al., 1985). This was confirmed by Putaux, Buléon, and Chanzy (2000) who investigated the aging and aggregation of very dilute amylose and amylopectin dispersions with transmission electron microscopy. However, similar to the SANS work cited above on amylose gels, Suzuki et al. used the concept of fractal phases to interpret the SAXS of rather highly concentrated aqueous *starch* suspensions (Suzuki, Chiba, & Yano, 1997; Vallera et al., 1994). Clearly, also in the literature dealing with starch gelation, concepts of amylose aggregation or crystallization are as frequently occurring as phase separation concepts in a rather confusing way. This called for further research.

In the present study, the structural changes responsible for the viscosity changes in heat treated and sheared wheat starch–water mixtures are characterized during pasting and gelation through combined rheology and time-resolved X-ray scattering experiments using Couette cells. This work also addresses the influence of adding short-chain amylose–lipid complexes to aqueous starch dispersions. This item is included as a previous study by Putseys et al. (2010) has indicated significant changes in starch viscosity when analysing starch–water systems supplemented with either pure glycerol monostearate (GMS) or short-chain amylose–GMS complexes with a Rapid Visco-Analyzer (RVA). Characterising the associated structural aspects may highlight certain features and contribute to a general understanding of starch gelation.

2. Materials and methods

2.1. Materials

All chemicals, solvents and reagents were of at least analytical grade and from Sigma–Aldrich (Bornem, Belgium) unless specified otherwise. Potatoes were purchased on the local market. A commercial wheat starch sample was from Syral (Aalst, Belgium).

2.2. Methods

2.2.1. Synthesis of amylose–glycerol monostearate complexes

Potato phosphorylase was extracted from Nicola potatoes (*Solanum tuberosum cv. Nicola*) according to Gelders, Goesaert, and Delcour (2005). Defatted amylose–GMS complexes with typical differential scanning calorimetry dissociation temperatures of 100 °C were synthesized semienzymically as described elsewhere (Putseys et al., 2010).

2.2.2. Starch rheology

Rheology studies were performed with a Physica MCR 301 rheometer (Anton Paar, Graz, Austria). Mixed aqueous wheat starch dispersions (12 mL water; 8.0% starch dry matter, dm, without and with addition of 1.0% pure, *i.e.* uncomplexed, GMS or 5.0% defatted amylose–GMS complexes; percentages expressed as w/w, calculated on starch dm) were added to a Couette measuring system (Macosko, 1994). A sufficiently high starch concentration, *i.e.* 8.0% (w/w), was selected as to reach a space filling arrangement of swollen granules during the pasting process (the minimum concentration is around 6.0%, evidence available but not shown). Surpassing this stage avoids effects on the viscosity related to the volume occupied by the starch granules or remnants thereof.

The Couette system consists of an outer stationary cup (radius 14.46 mm) and an inner rotating bob (radius 13.33 mm). The small measuring gap (1.13 mm) ensures a constant shear rate throughout the gap. The gap length of 40 mm leads to a large contact area between sample and geometry which is beneficial for samples of low viscosity. A layer of mineral oil on top of sample and geometry prevented water evaporation. The dispersions were equilibrated for 2 min at 40 °C, heated to 95 °C at a rate of 5 °C/min and kept at this temperature for 10 min. Afterwards, the mixtures were cooled to 40 °C at 5 °C/min, and this temperature was held for 20 min. During the initial equilibration, the rotor speed was adjusted to result in a shear rate of 194.6 s^{-1}, while, from the heating phase onwards, it was 34.6 s^{-1} throughout the rest of the run. The rotor speeds and time–temperature profile were comparable to those commonly used for starch samples in RVA, as described by Putseys et al. (2010). At specific points in the temperature regime, shear was stopped for 30 s, to allow dynamic tests for on-line measurement of storage (G') and loss moduli (G''), expressed in Pa. The oscillatory strain was 1.0% in order to be in the linear viscoelastic domain, and the frequency, ω, was 1.0 Hz.

2.2.3. Time–temperature resolved small angle X-ray scattering and wide angle X-ray diffraction

In situ simultaneous SAXS and WAXD experiments were performed at DUBBLE, the Dutch-Belgian beam line (BM26) at the European Synchrotron Radiation Facility (ESRF; Grenoble, France) using a wavelength of 1.033 Å. The samples were placed in a polycarbonate Couette cell that allows X-ray access. The cell geometry is identical to that described by Pople, Hamley, and Diakun (1998), with modifications for temperature control by air powered heating guns (Homminga, Goderis, Hoffman, Reynaers, & Groeninckx, 2005) to be able to apply the same temperature–shear rate program as in rheometry.

The starch samples were weighed and slurried in deionized water [required dm content of 8.0% (w/w)]. Of such dispersions, 5.5 mL was transferred to the Couette cell. The samples were heated from 25 °C to 95 °C at 5 °C/min and then kept at this temperature for 10 min. They were then cooled to 40 °C at a cooling rate of 5 °C/min, and this temperature was held for 20 min. At the beginning of the temperature program, the shear rate was set to 300 s^{-1} and the bob of the Couette cell was gently moved up and down in the cup to prevent starch precipitation. This initial shear rate – chosen to make sure no starch precipitation occurred – is higher than the one used in the rheometry experiments. Explorative tests (data not shown) demonstrated that the initial shear rate does not affect the overall starch pasting (and gelation) processes. At 75 °C (during heating), a temperature above the gelatinization temperature of the starch sample, the shear rate was lowered to the same value as in the rheology experiments (34.6 s^{-1}). Up to this stage, no X-ray patterns were collected. X-ray patterns were only collected consecutively every 12 s starting as soon as the temperature had reached 95 °C. The 12 s acquisition time results in a scattering pattern every 1 °C during the cooling segment. In fact, the X-ray characterization only started once the granules are swollen and fill the whole space, as to be able to – at least from this perspective – treat the SAXS data in terms of a homogeneous system.

The SAXS patterns were measured on a two-dimensional (2D) multiwire gas-filled detector placed at 3.0 m from the sample. The data were averaged azimuthally using the home-made ConeX software (Gommes & Goderis, 2010) and are expressed as the intensity as a function of the scattering vector modulus $q = 4\pi/\lambda \sin(\theta/2)$, with λ being the wavelength and θ the scattering angle. The SAXS pattern of a water-filled Couette cell at the corresponding temperature was subtracted as a background after normalization of both patterns by the intensity of the beam measured by an ionization chamber downstream from the sample. The measured q-range spans from 0.2 nm^{-1} to 1.5 nm^{-1}, roughly corresponding to length scales ($d = 2\pi/q$) ranging from 4 to 30 nm. The reflections of silver behenate were used to calibrate the scattering angles (Huang, Toraya, Blanton, & Wu, 1993).

WAXD data were collected on a two-dimensional VHR Photonic Science (East Sussex, United Kingdom) CCD detector. The scattering angles were calibrated using a poly(ethylene) standard and, expressed in terms of q, cover the range $6\ nm^{-1} < q < 39\ nm^{-1}$. The patterns were normalized to the intensity of the incoming beam, corrected for the detector response and the dark current prior to being averaged azimuthally (Gommes & Goderis, 2010). Although WAXD data were collected, they are not discussed here since no noteworthy changes were observed at any stage during the imposed time–temperature–shear program. The WAXD data only revealed the liquid-like scattering due to the amorphous polymeric sample holder and the amorphous starch molecules in solution. No crystalline reflections were observed.

3. Results

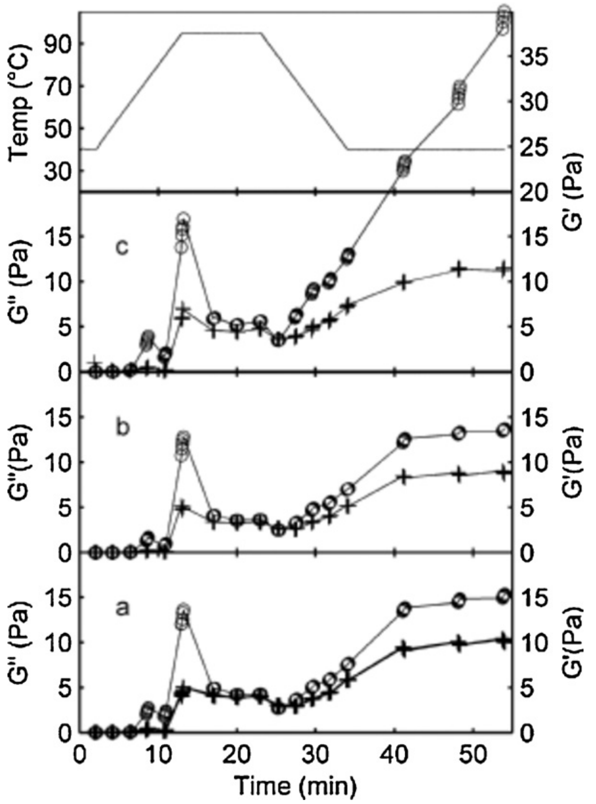

Fig. 1. Storage (G', ○) and loss (G'', +) moduli of starch pastes subjected to a temperature profile in a Couette cell with (a) 8.0% starch; (b) 8.0% starch + 1.0% glycerol monostearate (GMS); and (c) 8.0% starch + 5.0% amylose–GMS complexes.

Fig. 1 shows the storage (G') and loss (G'') moduli of the 8.0% starch dispersions without and with the different additives (1.0% pure GMS or 5.0% amylose–GMS complex), measured in the Couette cell rheometer. Both G' and G'' increase during the first heating segment with G' rapidly overtaking G'' indicating that a more solid-like behavior and, thus, a network is formed early on (Larson, 1999). Ultimately, 8.0% starch dispersions reach a space filling arrangement of swollen starch granules. When approaching the 95 °C isothermal segment, G' collapses whereas G'' hardly changes. During cooling, both G' and G'' rise with the increase of G' being most pronounced. G' increases further during the treatment at 40 °C and most spectacularly for the sample supplemented with amylose–GMS complex. The sample with pure GMS, on the other hand, hardly differed from the starch reference throughout the time–temperature profile.

For all samples, G' also tended to increase during the probing times when shearing was stopped and an oscillatory analysis was made. This increase in G' in the course of the 30 s probing was particularly clear at the highest G' values for the sample containing amylose–GMS complex.

Fig. 2 represents typical SAXS patterns, on a double logarithmic scale, obtained from the 8.0% pure starch dispersion. Note that in the SANS data by Vallera et al. (1994) clearly a power law behavior was present, which was interpreted as being due to a polymer-rich phase with a fractal dimension (d_f) of 2.6 and subunits with an estimated size between 17 and 20 nm, based on the high angle limit of the mass fractal regime in the SANS patterns. Beyond this high angle limit, a so-called Porod regime appeared, which is indicative of phases with sharp interfaces. Although our SAXS intensities display a continuous curvature with no clear power-law scattering and, in particular, no Porod regime, we rigorously followed the earlier work on starch or amylose gels (Suzuki et al., 1997; Vallera et al., 1994) and fitted the SAXS data with the following fractal

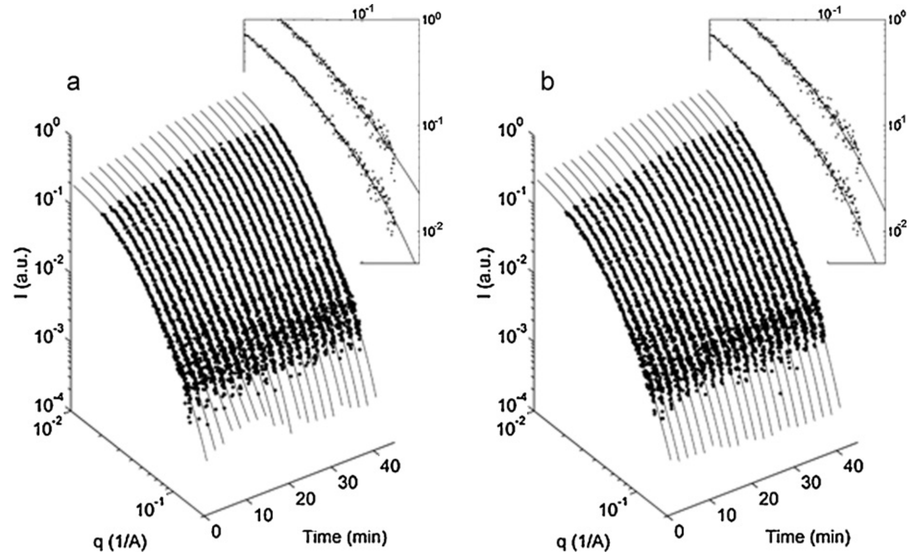

Fig. 2. Time–temperature-resolved SAXS patterns of the 8.0% starch dispersion fitted (a) with the fractal model, and (b) with the blurred cylinder model. The graphs at the right top corner are details of the fits for the first (top) and last (bottom) frames.

model (Pedersen, 1997; Teixeira, 1988)

$$I(q)=\frac{I_0}{\Gamma(d_f-1)(\xi/R_g)^{d_f}}\left\{1+\frac{d_f\Gamma(d_f-1)}{(qR_g)^{d_f}}\frac{\sin[(d_f-1)\tan^{-1}(q\xi)]}{[1+1/(q\xi)^2]^{(d_f-1)/2}}\right\}\exp\left(-\frac{(qR_g)^2}{3}\right) \qquad (1)$$

where I_0 is the scattered intensity extrapolated to angle zero, Γ is the gamma function, d_f is the fractal dimension, ξ is the upper cut-off length of the fractal aggregates, and R_g is the radius of gyration of the fractal's primary particles. In Eq. (1), the form factor of the primary particles is approximated by a Guinier function. This was justified because of the absence of Porod scattering in the measured q-range, meaning that – in the context of this model – the particles were smaller than the present SAXS resolution.

The solid lines in Fig. 2a are the least-square fits of the SAXS data with Eq. (1), with I_0, ξ and R_g as adjustable parameters, and $d_f = 2.6$. The latter value is justified based on previous SANS work on amylose gels (Vallera et al., 1994). The fractal modeling gives an acceptable fitting of the entire scattering pattern. Fig. 3a–c shows the time evolution of the fitted parameters for all samples. The results show a small and gradual increase in ξ with time, which levels off during the final holding phase. R_g decreases during the phase at 95 °C, but increases drastically (except for the sample containing 5.0% amylose–GMS complex) during cooling to end up at a value similar to that of the starting material. It needs to be mentioned that the R_g values, which represent the size of the fractal's primary particles, are consistently smaller than the SAXS resolution. These values are not very stable (and equally unreliable) as they only affect the patterns (via a small curvature in a double logarithmic plot) at the high q-side where the scattered intensity is relatively low. This holds in particular for the initial very low R_g values. I_0 remains rather constant during the isothermal phases at 95 and 40 °C, but increases during the cooling phase in between. The sample containing 5.0% amylose–GMS complex, however, increases more strongly during cooling. It is also conspicuous that I_0 follows the same pattern as G' and G'', except for G' in the sample with amylose–GMS complex in which the increase of I_0 is less spectacular.

Alternatively, and based on *e.g.* the SAXS work by I'Anson et al. (1988) and the microscopy results by Putaux et al. (2000), the SAXS curves deserve analysis in terms of a collection of cylindrical objects (aggregated amylose double helices). However, the absence in the experimental scattering patterns of any Porod region with exponent −4 rules out the presence of objects with sharp interfaces. Instead, the rigid elongated objects seem to be characterized by a more continuous variation of the electron density across their boundaries. From a SAXS point of view, such objects are conveniently modeled as the convolution of infinitely thin rods with an appropriate blurring function $b(r)$. In the reciprocal space, the convolution converts to a product between the respective Fourier transforms. Therefore, the SAXS intensity of such a morphological model is

$$I(q)=I_0\left[2\frac{Si(qL)}{qL}-4\left(\frac{\sin(0.5qL)}{qL}\right)^2\right]\left|B(q)\right|^2 \qquad (2)$$

where the bracketed term is the form factor of infinitely thin rods of length L (Pedersen, 1997), $B(q)$ is the Fourier transform of the blurring function $b(r)$, and the prefactor I_0 has the same meaning as in Eq. (1). In the first factor of Eq. (2), the function $Si(x)$ is defined as

$$Si(x)=\int_0^x\frac{\sin(t)}{t}dt \qquad (3)$$

which is also referred to as the sine integral function.

Several blurring functions were tried for analysis of the SAXS patterns. In particular, no satisfactory fit could be obtained with $B(q)$ modeled as a conventional Gaussian. The simplest function that enabled to fit all data nicely is an exponential function of the form

$$B(q)=\exp(-\sigma q) \qquad (4)$$

where the parameter σ, having the dimension of a length, characterizes the spatial extension of the electron density of the scatterers. The solid lines in Fig. 2b are least-square fits of the SAXS data with Eq. (2), with I_0, L and σ as adjustable parameters. The blurred cylinder model accounts for the entire scattering patterns of the investigated samples, including the large angle region, with only three adjustable parameters, as opposed to the fractal model which involves four parameters in the most general case where d_f would also have been varied during the fit.

Fig. 3d–f plots the fitted values of parameters I_0, L and σ. The most drastic changes occur in I_0, which almost doubles during cooling of the starch dispersions. A clear increase of parameter σ is observed simultaneously, which means that – in terms of this

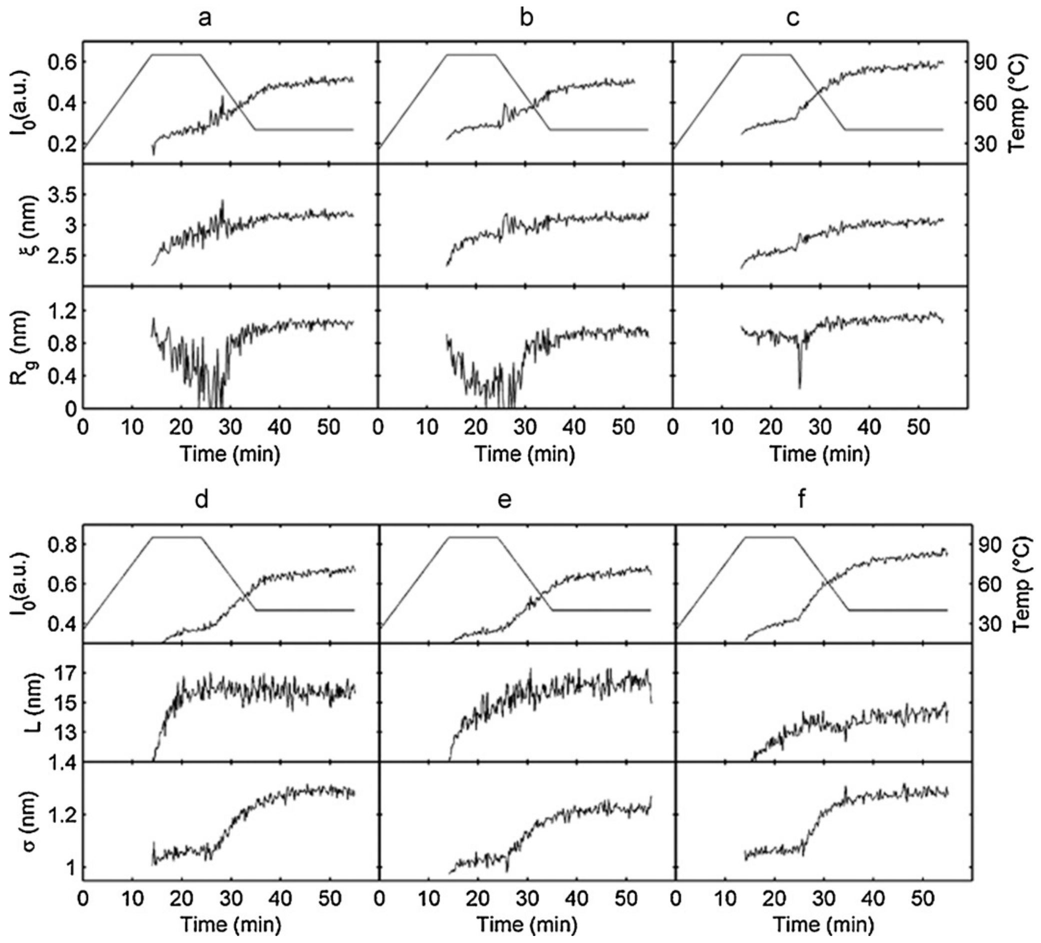

Fig. 3. *Top*: Time evolution of the fractal model parameters obtained from the SAXS data – extrapolated intensity scattered at zero angle (I_0), upper cut-off size of the fractal structure (ξ), and radius of gyration of the building blocks (R_g) – in the starch reference sample (a), starch supplemented with 1.0% glycerol monostearate (GMS) (b) and starch supplemented with 5.0% amylose–GMS complexes (c). In all cases, the fractal dimension was set to $d_f = 2.6$. The smooth lines refer to the imposed temperature profile. *Bottom*: Time evolution of the blurred cylinder parameters obtained from the SAXS data – extrapolated intensity scattered at zero angle (I_0), length of the cylinder (L), and lateral size of the cylinder (σ) – in the starch reference sample (d), starch supplemented with 1.0% glycerol monostearate (GMS) (e) and starch supplemented with 5.0% amylose–GMS complexes (f). The smooth lines refer to the imposed temperature profile.

model – the structures responsible for the scattering expand laterally upon cooling of the sample. Also in this model, I_0 and σ follow the same pattern as G' and G'' during the cooling phase to and holding phase at 40 °C. The length of the cylinders, however, increases at the very beginning of the isothermal stage at 95 °C, but remains virtually constant during the subsequent cooling. Only the sample supplemented with amylose–GMS complex seemed to increase slightly further with time.

At the end of the temperature program, the sample supplemented with amylose–GMS complex, was held under shear for another 3 h at 40 °C. In RVA, the extension of the final holding phase of this sample induced severe increases of the viscosity (Putseys et al., 2010). During this longer holding phase, the SAXS only showed a slow evolution in the direction of slightly larger intensities (I_0), and larger sizes (R_g for the fractal model, or σ for the blurred cylinder model). Fig. 4 shows that the SAXS intensity exhibited rapid changes when the shear was stopped at the same temperature. The stop of the shearing resulted in a jump of the SAXS intensity (I_0), and of all characteristic sizes (ξ and R_g, or L and σ), which indicates that shearing prevented these structures to grow in size and/or in concentration. Since the low angle curvature in the SAXS patterns, which in the blurred cylinder model is associated with L and on which a proper estimate of I_0 relies, surpassed the low q-limit of the SAXS window after 12 min, no L or I_0 values are reported beyond that time. No crystalline reflections appeared in the WAXD signal at the stop of the shearing (data not shown) which suggests that these structures are poorly, or not, crystalline.

4. Discussion

4.1. Rheometry

The magnitude of the complex viscosity $\left(\sqrt{(G'/\omega)^2 + (G''/\omega)^2}\right)$ calculated from the rheometry data runs parallel to the earlier reported evolution in apparent viscosity determined with RVA when the same samples were subjected to an identical time–temperature profile (Putseys et al., 2010). However, in the earlier RVA study it was observed that GMS addition postponed pasting and decreased breakdown of the starch paste during the 95 °C isothermal holding phase, whereas in the present Couette cell study, the rheological behavior of the GMS supplemented system is indistinguishable from that of the reference. The effects in the RVA experiment for GMS supplemented systems were related to adsorption of GMS to the starch granules and to formation of amylose–lipid complexes (Putseys et al., 2010). The absence of any rheological effect in the Couette cell experiments points at the absence of such processes when flow conditions are well controlled, although the shear rate is nominally identical. Indeed, while a Couette geometry predominantly induces a horizontal movement in

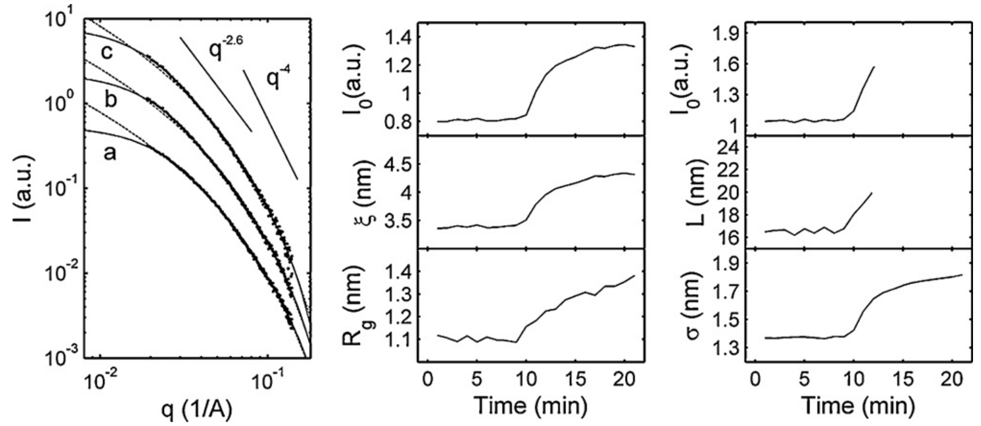

Fig. 4. *Left*: SAXS patterns measured before the stop of the shearing (a), 2 min after the stop (b), and 10 min after (c), together with the fits of the fractal model (solid line) and of the blurred cylinder model (dash). The *middle* and *right* panels show the continuous evolution of the fitted parameters; the shearing stopped at t = 10 min.

the sample (in absence of secondary Taylor vortices), the practical but rheologically complex RVA geometry is prone to induce more secondary flows. Be that as it may, this observation calls for further systematic work on the effects of shear rate, time and temperature using well controlled flow patterns such as can be realized with a Couette cell. Such work, however, is beyond the scope of the present paper.

When comparing the SAXS data with the rheological ones, it is worth recalling that the time-temperature program in Fig. 1 occurs under constant shear, but that the rheometry measurements of G' and G'' themselves were done under small-amplitude oscillations in absence of macroscopic shear. The increase of the SAXS parameters when shear was stopped (Fig. 4) thus also accounts for the static increases of G' observed at each point in Fig. 1.

4.2. Fractal structures or elongated scatterers

Although the work by Vallera et al. (1994) was our primary incentive to use fractal concepts, at this stage, the suggested two-phase fractal structure seems unrealistic because both ξ and R_g are extremely small. Vallera et al. mentioned fractal clusters of several micrometers with building blocks in the range between 17 and 20 nm, whereas we found cluster sizes of 3 nm (ξ) and building blocks of only 1 nm (R_g).

Alternatively, the evolution of the SAXS patterns – interpreted in terms of Eq. (1) – may be due to the scattering of individual polymer coils. The increase in I_0 during the *high temperature stage* can be attributed to an increasing concentration of amylose polymer coils that leach into the solution, and the increase in ξ in this scenario must imply that progressively larger amylose molecules are involved or that the coil configurations are expanding with temperature and/or time. As mentioned above, the fitted value of ξ at the end of the 95 °C segment is about 3 nm, which is converted to a hydrodynamic radius of the scatterers of $\xi\sqrt{d_f(d_f+1)/2} \approx 6.5$ nm (Teixeira, 1988). This value seems realistic when compared to the reported hydrodynamic radius (7 nm) of amylose from pea starch (Parker & Ring, 2001), which has a similar degree of polymerisation as wheat based amylose. In contrast, the evolution of the scattering patterns during the *cooling* of the starch dispersions is not easily interpreted in terms of the temperature dependent scattering by polymer coils. The observed increase in I_0 cannot be explained in terms of an increasing concentration of leached amylose chains, since no further leaching of amylose is expected during cooling. In fact, there is no reason why the amylose chains would selectively appear in the SAXS patterns of the homogenized starch paste, even not during heating. On these grounds, it seems that a SAXS interpretation in terms of dissolved polymer coils is unrealistic.

Ultimately, the absence of a linear region in double logarithmic representations of the scattering data with a slope equal to −2.6 (*i.e.* the negative fractal dimension, d_f, imposed in the fit) points to the highly artificial and unrealistic nature of this fractal approach, whatever the underlying morphological features are. The obtained values of ξ and R_g suggest a fractal structure made up of building blocks (R_g) that constitute a scatterer of only three times its size (ξ). This proximity of the two length scales is incompatible with the concept of fractal structures, implying morphological self-similarity over an extensive length scale range (Malcai, Lidar, Biham, & Avnir, 1997).

Therefore, a model consisting of a dilute dispersion of blurred cylinders was proposed. It allows fitting the data with only three adjustable parameters, the values of which are presented in Fig. 3d–f. Before discussing the fits of the SAXS with Eq. (2), it is useful to discuss the real-space structure corresponding to Eqs. (2) and (4). The mathematical details of this derivation are given in the Appendix. The inset to Fig. 5 shows the real-space structure of a

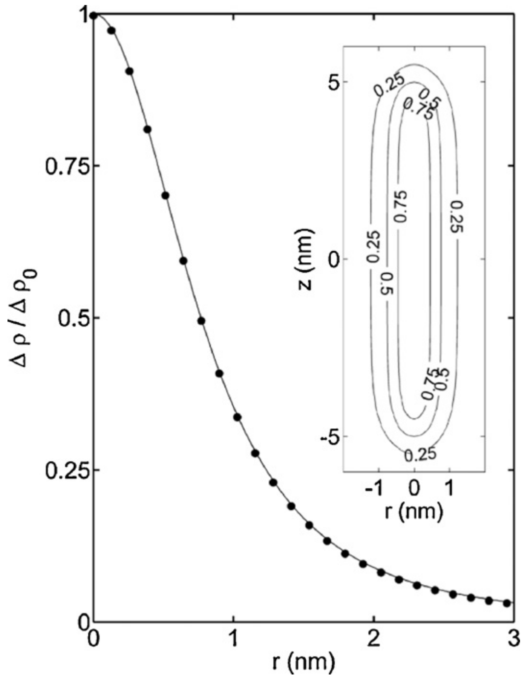

Fig. 5. Radial density profile $\Delta\rho(r)/\Delta\rho(0)$, for σ = 1 nm, in case of $L \gg r$, and in the inset an electron density map of a blurred cylinder with L = 10 nm and σ = 1 nm calculated from Eq. (2).

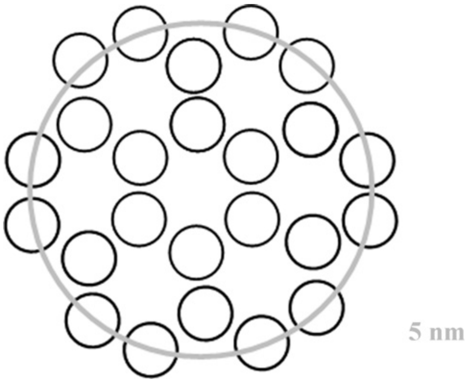

Fig. 6. Possible arrangement of amylose double helices in a B crystal type fashion within the cylindrical scattering objects. Small black circles represent cross-sections through the double helices (top view). The grey circle has a diameter of 5 nm.

blurred cylinder, scattering like Eq. (2) with $L = 10$ nm and $\sigma = 1$ nm. Fig. 5 shows the radial electron density profile $\Delta\rho(r)/\Delta\rho_0$ as a function of the distance to the cylinder axis for $\sigma = 1$ nm. Most of the structure is enclosed at a distance to the center smaller than 2σ. Although the actual diameter of such a blurred object is ill-defined, the value 4σ in the following will serve as a practical estimate of the diameter of the scatterers. It is worth pointing out that the blurriness of the structure may also reflect a diameter distribution, reducing the blurred nature of the actual individual scatterers.

The elongated structures detected by SAXS (see Fig. 3d–f) are about 15 nm in length and 5 nm in diameter. This diameter is significantly larger than that of single amylose double helices (*i.e.* about 1 nm) estimated from the structure of type B crystals (Parker & Ring, 2001). The suggested blurred cylinders are therefore to be understood as parallel aggregates of double helices. Fig. 6 illustrates a possible stacking of such double helices as seen in a cross-section through the cylinders and assuming a type B crystalline order, relying on the fact that this crystal type is formed when heated amylose chains crystallize upon cooling (Eerlingen, Crombez, & Delcour, 1993; Eliasson & Gudmundsson, 2006).

One may wonder why no crystalline reflections are observed in the scattering at wide angles if such arrangement would indeed be realistic. In principle, the amount of crystalline material might be too low and escape the WAXD sensitivity or, alternatively, the helices may not be stacked sufficiently regularly. In the latter case, the clusters could be called mesomorphic rather than crystalline. SAXS cannot discriminate between the options, but, in either case, if such objects would be present in the gel, they would dominate the SAXS signal over the contributions of dissolved amylose coils and other starch components – essentially amylopectin – in the mixture, as is explained in the next paragraph.

In 8.0% starch dispersions beyond the gelatinization temperature, the starch granules are swollen to such an extend that they fill the space completely (Steeneken, 1989). Furthermore, the polysaccharide concentration is so high that no single polymer coil scattering is expected. The polymer coils are interpenetrating and overlapping, resulting – together with the water – in a homogeneous liquid that only leads to a q-independent constant scattering at SAXS typical q-values (Hukins, 1981). This homogeneity can be disrupted as a result of liquid–liquid or liquid–solid phase separation processes. The electron density of the phases or objects will emerge from the continuous matrix and produce a SAXS signal on top of the background when the object or phase length scales are appropriate.

The suggested blurred cylindrical aggregates are very similar to the worm-like structures reported in numerous electron microscopy works on dried amylose gels. Our results also substantiate the earlier SAXS interpretation by I'Anson et al. (1988) who reported rod-like objects for amylose gels at rest, *i.e.* without the application of shear. That they found infinitely thin rods rather than (blurred) cylinders resulted – in their case – from the lack of SAXS data at high q-values where this information is present. Remarkably, the rod-like structures detected by I'Anson et al. are much longer (about 70 nm) than the blurred cylinders discussed in the present paper. This may result from the lower amylose level in our system. I'Anson et al. (1988) studied 6.0% amylose solutions, whereas the effective amylose concentration in our case is only 2.0% (±25% of an 8.0% starch solution). Furthermore, this length difference may be related to the presence of shear in our case, limiting the longitudinal growth of the cylindrical aggregates. The role that shear plays in hindering the growth of the aggregates is confirmed by the sudden increase in L and σ when shearing is stopped (Fig. 4).

However, when shearing is stopped, not only the size of the scattering objects increased suddenly, but also the shape of the SAXS patterns changed: the asymptotic slope of the patterns on a double log scale at relatively large q-values came closer to -4 (which is an indicator for sharp interfaces), and the low-angle scattering deviates from the blurred cylinder model (see curve c in Fig. 4). This possibly points to an evolution of the morphology towards the fractal two-phase structure described by Vallera et al. (1994). Although these authors reported well defined interfaces, it needs to be noted that scattering at high q-values, *i.e.* beyond $q = 0.1$ Å^{-1}, in their case was rather noisy and could not exclude blurred interfaces on the smallest length scales. In fact, Fig. 6 illustrates that interfaces of B-type crystals cannot be sharp down to the atomic level as they are made up of stacked double helices. The fractal phases reported by Vallera et al. (1994) consist of subunits with a size of 17–20 nm, which is significantly larger than the values $4\sigma \sim 7.0$ nm found at the end of the experiment depicted in Fig. 4, but which is very close to the estimated cylinder lengths. The increase of σ and L when shearing is stopped and the progressive departure from the adopted cylindrical model suggest that shearing – besides hindering longitudinal and lateral growth of the amylose double helix clusters – also prevents the further agglomeration of these clusters into fractal macro-aggregates.

4.3. Nanostructural analysis of gelation

The blurred scatterer model of SAXS brings semi-quantitative information on the number of cylindrical double helix aggregates and the total volume of these aggregates. The latter is proportional to the total amount of double helices involved in crystallization. Both are expected to influence the network formation and, thus also the rheology of the sample via the amylose chain fragments that bridge different clusters of double helices. In case of dilute dispersions, the SAXS intensity at angle zero, I_0, is proportional to $nV^2(\Delta\rho)^2$, where n is the number concentration of scatterers, V is their individual volume, and $\Delta\rho$ is their electron density contrast with the solvent (Pedersen, 1997). In our case, the volume of the scatterers V is proportional to $L\sigma^2$. If we further assume that the contrast of the scatterers with the solvent is a constant, and that only their size and concentration change with temperature and time, we can infer that the quantity $I_0/(L\sigma^2)^2$ is proportional to the concentration n of scatterers in the solutions (Gommes, Goderis, Pirard, & Blacher, 2007). This quantity, estimated from the SAXS parameters depicted in Fig. 4, is plotted in Fig. 7a against time for all three solutions.

The decrease of G' at the beginning of the 95 °C isothermal dwell seems to be mirrored in the evolution of $I_0/(L\sigma^2)^2$. In other words, aggregates formed at relatively low temperatures from the leached amylose chains during the heating phase, dissociate at higher temperature. Elaborating on this similarity with melting,

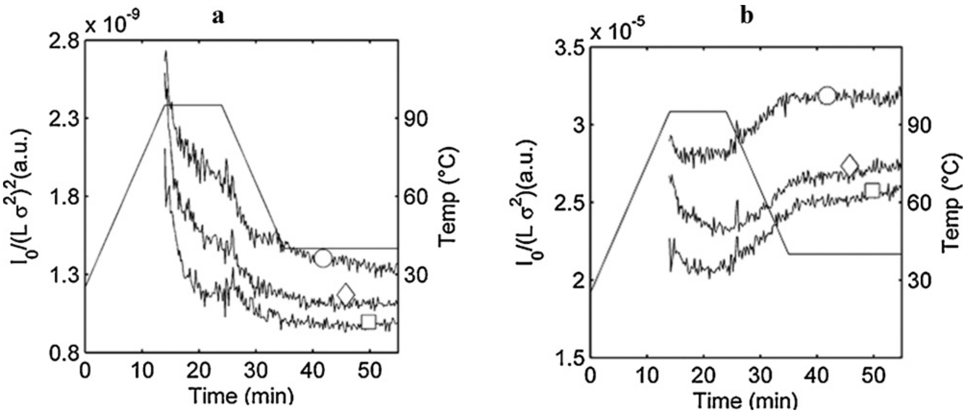

Fig. 7. (a) SAXS-based estimate, $I_0/(L\sigma^2)^2$, proportional to the concentration of double helix cylindrical aggregates for 8.0% starch (square); 8.0% starch + 1.0% glycerol monostearate (GMS) (diamond) and 8.0% starch + amylose–GMS complexes (circle), subjected to a time–temperature profile (smooth line) in a Couette cell. (b) SAXS-based estimate, $I_0/(L\sigma^2)$, proportional to the total volume occupied by the double helix cylindrical aggregates for 8.0% starch (square); 8.0% starch + 1.0% glycerol monostearate (GMS) (diamond) and 8.0% starch + 5.0% amylose–GMS complexes (circle), subjected to a time–temperature profile (smooth line) in a Couette cell.

and considering the results in Fig. 7a, we argue that the apparent increase of L (Fig. 3d–f) during the high temperature stage reflects the preferential melting of the smallest aggregates, rather than a growth of the existing ones. Only the largest ones survive the heat treatment. Relations between the crystal size and their melting temperature are conveniently cast into a Gibbs-Thomson equation with structural parameters and surface energies suited for a given (crystal) geometry (Wunderlich, 1980). Recently, a relation between the lamellar crystal thickness of amylose-rich starch samples and their melting temperature was established. According to the work by Gomand, Lamberts, Gommes, Delcour, and Goderis (submitted for publication), only large size amylose crystals are expected to melt at about 150 °C in excess water, which is an often cited melting temperature for mature amylose crystals (Delcour & Hoseney, 2010).

The further decrease of $I_0/(L\sigma^2)^2$ during the cooling has another origin. As it is accompanied by an increase of the lateral size σ of the aggregates (Fig. 3d–f), it is natural to envisage it as an agglomeration or ripening of existing aggregates into fewer, but larger structures. Such processes should leave the total volume of the aggregates unchanged. This seems not to be the case, as illustrated in Fig. 7b where the quantity $I_0/(L\sigma^2)$, proportional to the total volume of the aggregates, clearly increases. Therefore, besides the agglomeration and/or ripening of existing double helix aggregates also new aggregates seem to be nucleated and/or existing aggregates grow by the addition of doubles helices from the solution. In contrast, the decrease in the number of scatterers at high temperature leads to a decrease of their total volume (Fig. 7b), in line with the melting hypothesis.

Comparison of Figs. 1 and 7b shows that the temperature dependence of the gel stiffness, G', parallels the total volume of aggregates over the entire temperature range. In general, the granule volume fraction, granule stiffness and amylose aggregation determine the sample viscosity (Gomand et al., submitted for publication). In the present case, the swollen granules are space filling and, by shear force actions, they are undoubtedly disintegrated to a large extent leading to a homogenized material. The qualitatively similar evolution of G' and of $I_0/(L\sigma^2)$ clearly indicate that aggregated amylose double helices – although relatively small – are the main factor determining the rheology of the starch pastes under the homogeneous conditions studied here. In the isothermal segment at 40 °C, the total volume of the aggregates is constant, which is also reflected in a constant G' for two of the three samples, but clearly not in the dispersion supplemented with amylose–GMS complex, in which G' increases continuously. A similar evolution is seen in Fig. 7a, which reveals a small but continuous decrease of the concentration of aggregates of that particular solution during the isothermal dwell. At first sight, the accompanying constant total volume (Fig. 7b) points at processes driven by a tendency to reduce the interfacial area, such as crystal ripening or cluster coalescence. From this perspective, it seems natural to expect a *lateral* cluster growth, *i.e.* an increase in σ. However, careful inspection of the data (Fig. 3d–f) reveals that the increase of the cluster size ($\sim L\sigma^2$) in the isothermal part at 40 °C results from a small increase in L rather than in σ. We may speculate that longitudinal growth is hampered when the mobility of the leaving polymer chains is constrained by connectivity to other clusters and that it is energetically favorable to sacrifice a number of (small) clusters to release these constraints and to allow longitudinal growth. On the other hand, it is not obvious how this process can account for the concomitant spectacular increase of the stiffness of the network, *i.e.* G', as observed in Fig. 1. If this stiffness increase would not be a mere effect of size, it may well be that the nature of the clusters changes as a result of a change in the size. Changes in nature may involve size-induced polymorphic transitions or a transition from mesomorphic to crystalline order, which in turn may increase the stiffness of the clusters and, hence, of the gel-forming network. A clear example of such transition in synthetic polymers has been reported by Rastogi and Kurelec (2000) for polyethylene crystallizing at high pressure. They observed that small polyethylene crystals are initially formed in the hexagonal phase. Interestingly, in this mesomorphic phase, polymer chains can move parallel to the chain axis and crystal growth is allowed in the chain direction up to a critical size where the crystal structure converts into an orthorhombic packing. This transition locks in the crystal dimension in the chain direction and freezes all axial chain movements. Keller et al. (1994) published schemes on the size dependence of phase stabilities and Strobl (2006) casted these concepts into the broad context of polymer crystallization at ambient pressure.

Such processes – if they apply – seem not to occur for the other two solutions since no increase of G' is observed at 40 °C in their case. It is possible that the clusters already reached the critical L dimension for crystal conversion prior to the isothermal stage at 40 °C. Indeed, for the other two samples, L is markedly larger. The lower stiffness for these samples may simply reflect the lower concentration (Fig. 7a) and total volume of clusters (Fig. 7b). The number and volume of aggregates at any given temperature is largest for the solution supplemented with amylose–GMS complex. This sample contains 5.0% additional mass on starch dm base, *i.e.* ±20% additional short linear chains on amylose dm base, which could account for the higher concentration observed. The high number and volume of aggregates in this sample, however, also suggest a facilitated

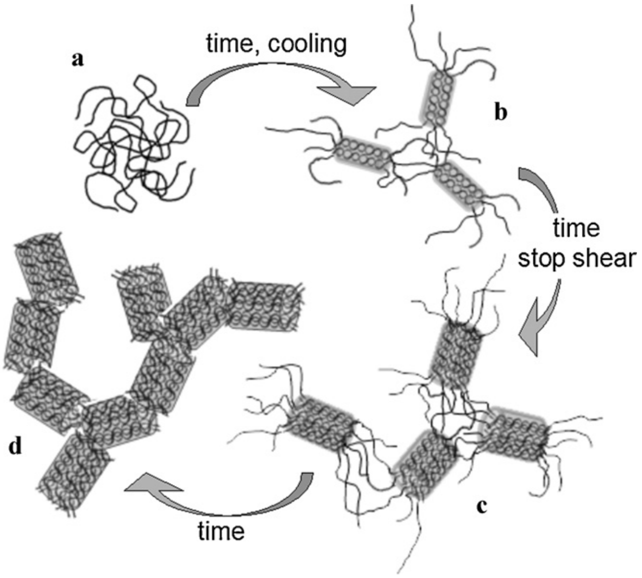

Fig. 8. Schematic overview of gelation of starch: amylose coils (a), leached out from the granule during and after gelatinization, form aggregates (b) especially during cooling of the heated starch dispersion. These aggregated structures are modeled by blurred cylinders. When shear is stopped, the cylinders increase in size and number (c). A further aggregation and clustering towards a fractal model with sharp interfaces (d), as suggested by Putaux et al. (2000) and Vallera et al. (1994), seems the logical following step. Note that this figure is only qualitative: the amount of double helices within the clusters might be significantly larger than shown.

aggregate nucleation induced by the freed short amylose fragments that – because of less conformational constraints – are more readily arranged into double helices in mutual conjunction or with fragments of the longer amylose chains leached from starch granules. However, a more efficient cluster nucleation may bring constraints to the polymer mobility, as discussed above, and hinder cluster growth and stabilization processes. Whether or not size-dependent crystal or double helix packing conversions are at hand cannot be decided from the present dataset since no obvious changes to the WAXD patterns could be observed for reasons mentioned above. In any case, the observed positive contribution of the short amylose chains to the viscosity build-up and the associated network formation corroborates earlier findings (Putseys et al., 2010).

In summary, during pasting and gelation of a starch dispersion, the following processes take place. First, amylose is released from the granules (Fig. 8a). These linear chains then interact by forming double helices, which aggregate to form a network. Network formation takes place immediately following starch gelatinization, since, from the beginning of pasting, the storage modulus is larger than the loss modulus. During cooling, existing aggregates of amylose double helices – modeled as blurred cylinders – aggregate and grow and new ones nucleate, leading to a stronger network and a larger viscosity (Fig. 8b). Stopping shear leads to further growth and clustering of the aggregates (Fig. 8c). It seems logical to consider these structures as precursors to the fractal structures (Fig. 8d) previously described by Vallera et al. (1994) and Putaux et al. (2000).

This line of thought may well resolve the inconsistency mentioned in the Introduction between the SAXS results by I'Anson et al. (1988) and the SANS data by Vallera et al. (1994), reporting, respectively, rod-like entities and two-phase fractal morphologies for amylose gels. The former data were recorded after quenching a hot amylose solution to room temperature, but it cannot be retrieved from their paper how long after the quench the gels were measured. It is likely that SANS data were collected considerably later than the time of the quench, thereby allowing ample time for helix cluster aggregation, and fractal morphologies to develop.

The suggested size-dependent crystallization pathways at this stage are rather hypothetical and call for further systematic research on, *e.g.* pure amylose solutions with suitable supplements. Combined SAXS/WAXD experiments involving shear are of particular interest since this seems to be a means to preserve the initial stages of crystallization whereas stopping shearing can be used to trigger further stabilization processes.

5. Conclusion

This study underlines the essential role of amylose in the rheological behavior of gelling aqueous starch solutions. Time-temperature resolved SAXS under shear clearly indicates that aggregated amylose double helices, modeled as thin blurred cylinders, are the primary determinants in starch gelation. The concentration and total volume of the amylose double helix aggregates determine the concomitant changes in rheology. Application of shear, however, inhibits growth of these aggregates. The increase in G' when supplementing the material with amylose–lipid complexes results from a larger concentration and total volume of cylindrical aggregates, each consisting of a higher level of double helices, brought about by the liberation of short amylose chains from the complex. Further research is needed to elucidate the origin of the spectacular increase in network stiffness during the holding time at 40 °C. It is suggested that size-induced polymorphic changes may play a role.

Acknowledgements

This publication is financially supported by the European Commission in the Communities 6th Framework Program, Project HEALTHGRAIN (FOOD-CT-2005-514008). It reflects the author's views and the Community is not liable for any use that may be made of the information contained in this publication. This research was also conducted in the framework of research project G.0427.07, financed by the Fund for Scientific Research – Flanders (FWO-Vlaanderen), Brussels, Belgium and is part of the Methusalem program "Food for the Future" at the K.U.Leuven. C.J.G is a postdoctoral researcher of the F.R.S.-FNRS, Belgium. The authors thank FWO-Vlaanderen for supporting the DUBBLE project.

Appendix A. Real-space structure corresponding to the blurred cylinder model

The blurred cylinder model we introduced to analyze the SAXS data is a convolution of a dilute dispersion of infinitely thin rods by a blurring function. In Fourier space, the convolution becomes a regular product, which leads to Eq. (2). In this appendix, we derive the real space structure of the electron distribution corresponding to an exponential blurring function in Fourier space.

The three-dimensional Fourier transform of Eq. (4) is calculated via classical calculus, and one finds

$$b(r) = \frac{\sigma}{\pi^2}(\sigma^2 + r^2)^{-2} \tag{A1}$$

The blurring function $b(r)$, given by Eq. (A1), describes how a point-wise electron density is blurred. The actual electron distribution corresponding to Eq. (2) is a convolution of Eq. (A1) with an infinitely thin rod of length L. In cylindrical coordinates (z, r), with z parallel to the rod, the electron density difference between the blurred cylinder and the pure solvent is therefore written as

$$\Delta\rho(z, r) = \frac{n_e}{L}\int_{-L/2}^{+L/2} \frac{\sigma}{\pi^2}[\sigma^2 + r^2 + (z - x)^2]^{-2}\, dx \tag{A2}$$

with n_e the total extra number of electrons in the blurred cylinder, compared to the same volume of solvent.

The inset in Fig. 5 shows the electron density map $\Delta\rho/\Delta\rho_0$ in the central plane of the blurred cylinder with $\Delta\rho_0 = n_e/(2\pi\sigma^2 L)$, for $L = 10$ nm and $\sigma = 1$ nm. The latter numerical values correspond roughly to those derived from the SAXS (see Fig. 3d–f).

In order to relate the parameter σ to the lateral size of the cylinders, it is convenient to consider the case $L \gg \sigma$. In this case, the electron density at a reasonable distance away from the cylinder apexes only depends on the radial distance to the center of the cylinder, and Eq. (A2) simplifies to

$$\frac{\Delta\rho(r)}{\Delta\rho_0} = \left(1 + \left(\frac{r}{\sigma}\right)^2\right)^{-3/2} \tag{A3}$$

with $\Delta\rho_0 = n_e/(2\pi\sigma^2 L)$. The electron density profile obtained from Eq. (A3) is plotted in Fig. 5. The total number of extra electrons at a distance to the center of the cylinder smaller than r, $\Delta n(r)$, is obtained by integrating Eq. (A3) in cylindrical coordinates. The answer is found to be

$$\frac{\Delta n(r)}{n_e} = 1 - \left(1 + \left(\frac{r}{\sigma}\right)^2\right)^{-1/2} \tag{A4}$$

from which it is seen that about 50% of the extra electrons are at a distance to the center smaller than 2σ.

References

Atwell, W. A., Hood, L. F., Lineback, D. R., Varriano-Marston, E., & Zobel, H. F. (1988). The terminology and methodology associated with basic starch phenomena. *Cereal Foods World*, *33*(3), 306–311.

Buléon, A., Colonna, P., Planchot, V., & Ball, S. (1998). Starch granules: Structure and biosynthesis. *International Journal of Biological Macromolecules*, *23*(2), 85–112.

Delcour, J. A., Bruneel, C., Derde, L. J., Gomand, S. V., Pareyt, B., Putseys, J. A., et al. (2010). Fate of starch in food processing: From raw materials to final food products. *Annual Review in Food Science and Technology*, *1*, 87–111.

Delcour, J. A., & Hoseney, R. C. (2010). *Principles of cereal science and technology*. St. Paul, MN, USA: AACC International.

Eerlingen, R. C., Crombez, M., & Delcour, J. A. (1993). Enzyme-resistant starch 1. Quantitative and qualitative influence of incubation time and temperature of autoclaved starch on resistant starch formation. *Cereal Chemistry*, *70*(3), 339–344.

Eliasson, A. C., & Gudmundsson, M. (2006). Starch: Physicochemical and functional aspects. In A. C. Eliasson (Ed.), *Carbohydrates in food* (pp. 391–467). New York, NY, USA: Taylor & Francis.

Gelders, G. G., Goesaert, H., & Delcour, J. A. (2005). Potato phosphorylase catalyzed synthesis of amylose–lipid complexes. *Biomacromolecules*, *6*(5), 2622–2629.

Gidley, M. J., & Bulpin, P. V. (1989). Aggregation of amylose in aqueous systems – the effect of chain-length on phase-behavior and aggregation kinetics. *Macromolecules*, *22*(1), 341–346.

Gomand, S. V., Lamberts, L., Gommes, C. J., Delcour, J. A., & Goderis, B. Multistep annealed potato (mutant) starches: Morphology, thermal stability and functionality. *Biomacromolecules*, submitted for publication.

Gommes, C. J., & Goderis, B. (2010). CONEX, a program for angular calibration and averaging of two-dimensional powder scattering patterns. *Journal of Applied Crystallography*, *43*, 352–355.

Gommes, C. J, Goderis, B., Pirard, J.-P., & Blacher, S. (2007). Branching, aggregation, and phase separation during the gelation of tetraethoxysilane. *Journal of Non-Crystalline Solids*, *353*(24–25), 2495–2499.

Homminga, D., Goderis, B., Hoffman, S., Reynaers, H., & Groeninckx, G. (2005). Influence of shear flow on the preparation of polymer layered silicate nanocomposites. *Polymer*, *46*(23), 9941–9954.

Huang, T. C., Toraya, H., Blanton, T. N., & Wu, Y. (1993). X-ray-powder diffraction analysis of silver behenate, a possible low-angle diffraction standard. *Journal of Applied Crystallography*, *26*, 180–184.

Hukins, D. W. (1981). *X-ray diffraction by disordered and ordered systems*. Oxford, NY, USA: Pergamon Press.

I'Anson, K. J., Miles, M. J., Morris, V. J., & Ring, S. G. (1988). A study of amylose gelation using a synchrotron X-ray source. *Carbohydrate Polymers*, *8*, 45–53.

Imberty, A., & Perez, S. (1988). A revisit to the three dimensional structure of B-type starch. *Biopolymers*, *27*, 1205–1221.

Jenkins, P. J., & Donald, A. M. (1998). Gelatinisation of starch: A combined SAXS/WAXS/DSC and SANS study. *Carbohydrate Research*, *308*(1–2), 133–147.

Juhasz, R., & Salgo, A. (2008). Pasting behavior of amylose amylopectin and their mixtures as determined by RVA curves and first derivatives. *Starch-Stärke*, *60*(2), 70–78.

Keller, A., Hikosaka, M., Rastogi, S., Toda, A., Barham, P. J., & Goldbeckwood, G. (1994). The size factor in phase-transitions – Its role in polymer crystal-formation and wider implications. *Philosophical Transactions of the Royal Society of London Series A: Mathematical Physical and Engineering Sciences*, *348*(1686), 3–17.

Larson, R. G. (1999). *Polymer gels. The structure and rheology of complex fluids*. New York, NY, USA: Oxford University Press., pp. 232–260.

Leloup, V. M., Colonna, P., Ring, S. G., Roberts, K., & Wells, B. (1992). Microstructure of amylose gels. *Carbohydrate Polymers*, *18*(3), 189–197.

Macosko, C. W. (1994). *Rheology: Principles, measurements and applications*. New York, NY, USA: John Wiley & Sons.

Malcai, O., Lidar, D. A., Biham, O., & Avnir, D. (1997). Scaling range and cutoffs in empirical fractals. *Physical Review E*, *56*(3), 2817–2828.

Miles, M. J., Morris, V. J., Orford, P. D., & Ring, S. G. (1985). The roles of amylose and amylopectin in the gelation and retrogradation of starch. *Carbohydrate Research*, *135*(2), 271–281.

Miles, M. J., Morris, V. J., & Ring, S. G. (1985). Gelation of amylose. *Carbohydrate Research*, *135*(2), 257–269.

Parker, R., & Ring, S. G. (2001). Aspects of the physical chemistry of starch. *Journal of Cereal Science*, *34*(1), 1–17.

Pedersen, J. S. (1997). Analysis of small-angle scattering data from colloids and polymer solutions: Modeling and least-squares fitting. *Advances in Colloid and Interface Science*, *70*, 171–210.

Pople, J. A., Hamley, I. W., & Diakun, G. P. (1998). An integrated Couette system for in situ shearing of polymer and surfactant solutions and gels with simultaneous small angle X-ray scattering. *Review of Scientific Instruments*, *69*(8), 3015–3021.

Putaux, J. L., Buléon, A., & Chanzy, H. (2000). Network formation in dilute amylose and amylopectin studied by TEM. *Macromolecules*, *33*(17), 6416–6422.

Putseys, J. A., Derde, L. J., Lamberts, L., Östman, E., Björck, I. M., & Delcour, J. A. (2010). Functionality of short chain amylose–lipid complexes in starch–water systems and their impact on in vitro starch degradation. *Journal of Agricultural and Food Chemistry*, *58*, 1939–1945.

Rastogi, S., & Kurelec, L. (2000). Polymorphism in polymers: Its implications for polymer crystallisation. *Journal of Materials Science*, *35*(20), 5121–5138.

Steeneken, P. A. M. (1989). Rheological properties of aqueous suspensions of swollen starch granules. *Carbohydrate Polymers*, *11*, 23–42.

Strobl, G. (2006). Crystallization and melting of bulk polymers: New observations, conclusions and a thermodynamic scheme. *Progress in Polymer Science*, *31*(4), 398–442.

Suzuki, T., Chiba, A., & Yano, T. (1997). Interpretation of small angle X-ray scattering from starch on the basis of fractals. *Carbohydrate Polymers*, *34*, 357–363.

Teixeira, J. (1988). Small-angle scattering by fractal systems. *Journal of Applied Crystallography*, *21*, 781–785.

Tester, R. F., & Debon, S. J. J. (2000). Annealing of starch – A review. *International Journal of Biological Macromolecules*, *27*(1), 1–12.

Tester, R. F., Karkalas, J., & Qi, X. (2004). Starch – Composition, fine structure and architecture. *Journal of Cereal Science*, *39*(2), 151–165.

Tester, R. F, & Morrison, W. R. (1990). Swelling and gelatinization of cereal starches. 1. Effects of amylopectin, amylose, and lipids. *Cereal Chemistry*, *67*(6), 551–557.

Vallera, A. M., Cruz, M. M., Ring, S. G., & Boué, F. (1994). The structure of amylose gels. *Journal of Physics: Condensed Matter*, *6*, 311–320.

Waigh, T. A., Gidley, M. J., Komanshek, B. U., & Donald, A. M. (2000). The phase transformations in starch during gelatinisation: A liquid crystalline approach. *Carbohydrate Research*, *328*(2), 165–176.

Wang, T. L., Bogracheva, T. Y., & Hedley, C. L. (1998). Starch: As simple as A, B, C? *Journal of Experimental Botany*, *49*(320), 481–502.

Wunderlich, B. (1980). *Macromolecular physics. Vol. 3. Crystal melting*. New York, NY, USA: Academic Press.